Optical and structural characterization of Ge clusters embedded in ZrO_2

E. Agocs[a], Z. Zolnai[a], A. K. Rossall[b], J. A. van den Berg[b], B. Fodor[a],
D. Lehninger[c], L. Khomenkova[d], S. Ponomaryov[d], O. Gudymenko[d],
V. Yukhymchuk[d], B. Kalas[a], J. Heitmann[c], P. Petrik[a]

[a]Institute for Technical Physics and Materials Science (MFA), Center for Energy
Research (EK), Hungarian Academy of Sciences (MTA), Konkoly Thege Rd. 29-33, 1121
Budapest, Hungary
[b]International Institute for Accelerator Applications (IIAA), School of Computing and
Engineering, University of Huddersfield, Huddersfield, HD1 3DH, UK
[c]Institute of Applied Physics, TU Bergakademie Freiberg, D-09596 Freiberg, Germany
[d]V. Lashkaryov Institute of Semiconductor Physics, 45 Pr. Nauky, Kyiv 03028, Ukraine

Abstract

The change of optical and structural properties of Ge nanoclusters in ZrO_2 matrix have been investigated by spectroscopic ellipsometry versus annealing temperatures. Radio-frequency top-down magnetron sputtering approach was used to produce the samples of different types, i.e. single-layers of pure Ge, pure ZrO_2 and Ge-rich-ZrO_2 as well as multi-layers stacked of 40 periods of 5-nm-Ge-rich-ZrO_2 layers alternated by 5-nm-ZrO_2 ones. Germanium nanoclusters in ZrO_2 host were formed by rapid-thermal annealing at 600-800 °C during 30 s in nitrogen atmosphere. Reference optical properties for pure ZrO_2 and pure Ge have been extracted using single-layer samples. As-deposited multi-layer structures can be perfectly modeled using the effective medium theory. However, annealed multi-layers demonstrated a significant diffusion of elements that was confirmed by medium energy ion scattering measurements. This fact prevents fitting of such annealed structure either by homogeneous or by periodic multi-layer models.

Keywords:
Spectroscopic Ellipsometry, Ge nanoclusters, ZrO_2, RF magnetron sputtering, Medium energy ion scattering

1. Introduction

Semiconductor or metallic nanocrystals (NCs) embedded in dielectric matrices have been widely studied over the last decade [1, 2, 3, 4]. Specifically, Si and Ge nanocrystals are discussed as absorbers for third generation solar cells [5], as sensitizers of rare earth elements [6, 7], as light emitters [8] and as charge storage node in non-volatile memory devices [1, 9, 10]. Among Ge-rich oxide materials, the main attention was paid to the Ge-NCs embedded in SiO_2, whereas the Ge-NCs formed in Si_3N_4, Al_2O_3, HfO_2 were less addressed. Recently, a promising application of Ge-NCs embedded in ZrO_2 matrix for nanocrystal-based flash memory devices has been shown [10], since Ge has a smaller band gap than Si, and ZrO_2 has a higher k value than SiO_2 that increases the electric field across the tunneling oxide. This material system may also be interesting for third-generation solar cells, since Ge has a higher exciton Bohr radius. Therefore, a stronger quantum confinement effect is expected than for e.g. Si nanocrystals, and the band gap can better be adjusted.

Although such nanocrystal-based structures can be investigated using different thin-film characterization methods, among optical methods ellipsometry was shown to be very capable for nanocrystal measurement [11, 12, 13, 14] providing numerous advantages. The high sensitivity combined with the high speed and the non-destructive nature results in two main capabilities: (1) The sample properties can be quickly and non-destructively qualified as well as mapped on large surfaces; (2) Based on the non-destructive nature and the *in situ* application, there is a possibility to follow the transformation of the sample structure during deposition and/or annealing. Even though such optical measurements can be performed, a suitable analysis can be completed only if proper optical models have been developed and accurate reference dielectric functions exist.

The present study has two major aims. First, to develop and to test proper optical models to determine Ge nanocrystals in a single Ge-rich-ZrO_2 layer as well as in a multi-layer structure. Second, to demonstrate the validity of this method by the optical investigation of the evolution of the samples structure caused by annealing. The optical characterization is very challenging since the samples contain mixed phases, and the dielectric functions of the constituents are changing with the annealing conditions and stack-depth. To determine the volume fraction of the phases as well as to follow the phase separation and the changes in the crystalline structure of the Ge

2

phase accurately, the Bruggeman effective medium approximation (B-EMA) was applied. For this purpose the optical properties (dielectric functions) determined separately for pure Ge, pure ZrO_2 and Ge-rich-ZrO_2 single-layers produced with the same deposition conditions as multi-layer structures, were used.

2. Experimental details

The samples were fabricated using a radio-frequency (RF) magnetron sputtering system equipped with a confocal arrangement of 3-inch targets (Ge, ZrO_2 and SiO_2). Pure Ge, pure ZrO_2 and composite Ge-rich-ZrO_2 single-layers (left-hand side of Fig. 1) as well as [pure Ge/pure ZrO_2]$_{40}$ (denoted as Sample 'Ge' later on) and [Ge-ZrO_2/ZrO_2]$_{40}$ (denoted as Sample 'Ge-ZrO_2') multi-layers consisting of 40 periods of alternating Ge (or Ge-rich-ZrO_2) and ZrO_2 layers, each 5 nm thick (right-hand side of Fig. 1), were deposited on Si wafers covered by 5 nm thermal silicon oxide layer . The samples were capped also by a 20-nm silicon oxide layer produced by RF sputtering to prevent outward diffusion of Ge during annealing. For the samples investigated in this study, RF power densities of 1.6 W/cm^2 and 3.3 W/cm^2 were used for the Ge and ZrO_2 targets, respectively, providing a nominal composition of about 50 at.% for the Ge content in the Ge-rich-ZrO_2 composite layers.

The ellipsometric measurements were performed by means of a Woollam M-2000DI rotating compensator ellipsometer in the wavelength range of 190-1690 nm in 706 points at angles of incidence of 65°, 70° and 75°. The CompleteEASE software was used to evaluate the ellipsometric spectra using all the incident angles for the fit, although in most figures we only present the data at 70°, for the sake of better visibility.

Raman scattering spectra were excited with a 488.0-nm line of an Ar$^+$ laser and recorded using a LabRam HR800 micro-Raman system equipped with a Peltier-cooled CCD detector. All measurements were performed in the backscattering geometry. The power of the laser excitation was chosen to prevent the heating of the samples.

The as-deposited and annealed 'Ge-ZrO_2' samples were analyzed by medium energy ion scattering (MEIS) at the IIAA, Huddersfield, using 100-keV He$^+$ ions scattered through an angle of 90° and detected with a toroidal electrostatic ion analyzer. The spectrum edges of Zr and Ge in the first and second sublayers and Si and O in the surface silicon dioxide layer are indicated by

3

arrows in Fig. 2. The measured data were modeled by RBX spectrum simulations [15]. This modeling appropriately matched the experimental data to yield compositions of the top surface of the multilayer sample. Due to the limited information depth for the He$^+$ ions the model consists of only 6 layers represented the near-surface region of the sample. The first layer describes the oxide film, the second, fourth and sixth describe the ZrO$_2$ layers and the third and fifth represent the Ge-ZrO$_2$ composite layers, respectively.

The concentration depth profile of the samples was obtained on the scanning Auger microprobe JAMP-9500F of JEOL production (Japan) with the spatial resolution in the secondary electron image mode of 3-nm. The instrument is equipped with the hemispherical Auger electrons analyzer with the energy resolution $\Delta E/E$ of 0.05 to 0.6% and the ion gun for the layer-by-layer analysis with an Ar$^+$ ion beam diameter of 120 μm that is able to raster 1×1 mm. The variation range of Ar$^+$ ion beam energy is from 0.01 to 4 keV, while the minimal beam current is 2 μA at 3 keV. The vacuum of the specimen chamber was better than $5 \cdot 10^{-7}$ Pa.

X-ray diffraction data were collected with a Philips X'PERT apparatus using Cu K$_\alpha$ radiation in the range of $2\Theta = 20 - 80°$ using grazing geometry. An asymmetric grazing geometry was chosen to increase the volume of material interacting with X-ray beam, as well as to reduce the contribution from the Si substrate. The data were compared with standard cards of Powder Diffraction File Database (#37-1484 for monoclinic ZrO$_2$, #50-1089 for tetragonal ZrO$_2$, #4-0545 for cubic Ge). All measurements were performed at room temeprature.

3. Results and discussion

References for both ZrO$_2$ and pure Ge were determined on single-layer samples prepared with the same deposition conditions as those used for multilayer structures. The dielectric function of the ZrO$_2$ component was described by the Cauchy parametrization in the form of

$$n(\lambda) = A + \frac{B}{\lambda^2} + \frac{C}{\lambda^4}, \tag{1}$$

$$k(\lambda) = A_k \cdot e^{Exp \cdot (E - E_b)}, \tag{2}$$

where λ denotes the wavelength in μm, and A, B, C, A_k (amplitude) and E_b (band edge) are the Cauchy parameters of the real (n) and imaginary

4

(k) parts of the complex refractive index. The layer structure consists of a Si(substrate) / ZrO_2 / SiO_2(capping layer) stack with Si and SiO_2 reference values taken from the literature [16]. The fit results for the Cauchy parameters of the as-deposited ZrO_2 were $A = 1.988$, $B = 0.0092$ μm^2 and $C = 0.000812$ μm^4. (The error of the fit on all the Cauchy paramteres is less than 1%.) The Cauchy parameters for k (A_k and Exp) were only fitted (with E_b kept constant) to check the absorption, resulting in $k = 0$, as expected. The refractive index variation for the as-deposited and annealed single-layer ZrO_2 samples is plotted in Fig. 3.

To extract the parameters for single-layer Ge samples, the same stack as for the ZrO_2 layers was used. However, being a semiconductor, germanium requires more complex parameterization of the dielectric function for the modelling. For the as-deposited Ge layer the Urbach-Cody-Lorentz parameterization was used, assuming an amorphous material:

$$\epsilon_2(E) = \frac{E_1}{E} exp\Big(\frac{E - E_g - E_t}{E_u}\Big) \quad , \quad 0 < E \leq E_g + E_t \tag{3}$$

$$\epsilon_2(E) = G(E)L(E) \quad , \quad E > E_g + E_t, \tag{4}$$

where $G(E)$ is the near-bandgap function:

$$G(E) = \frac{(E - E_g)^2}{(E - E_g)^2 + E_p^2}, \tag{5}$$

$L(E)$ is the Lorentz oscillator function:

$$L(E) = \frac{AE_0\Gamma E}{(E^2 - E_0^2)^2 + \Gamma^2 E^2}, \tag{6}$$

and E_1 is defined as

$$E_1 = (E_g + E_t)G(E_g + E_t)L(E_g + E_t), \tag{7}$$

where E_g denotes the bandgap, A is the amplitude, E_0 is the peak transition energy and Γ the broadening term of Lorentz absorption peak. E_p and E_t denote the farther two transition energies. The dielectric function of Ge determined by fitting the parameters of the above equations are shown in Fig. 4 together with other references from the literature. The fact that the dielectric function of a-Ge differs from that of the literature is consistent with results of amorphous Si, showing the dependence of dielectric function

5

of amorphous semiconductors on the preparation conditions [17], which can partly be attributed to the presence of a micro- and nanocrystalline component [18]. The dependence of structural and optical properties of Ge on the preparation conditions and the thickness has also been shown for Ge in many works including the investigation of rf glow-discharge deposited [19], ion implantation amorphized [20], multi-layered [21], gold mediated [22], and a range of other non-single crystal Ge structures. The studies reveal significant differences depending on the preparation methods, and parameters including layer thickness [23].

The superlattice samples have been modeled using either a single-layer (MsL) or a multi-layer (MmL) approach. Both of them utilize a layer stack of Si(substrate) / SiO_2 / SL / SiO_2, whereas the 'MsL' and the 'MmL' models use a B-EMA layer and 40 pairs of B-EMA layers, respectively, describing the superlattice (SL) structure (see Fig. 1). In the B-EMA layer, we used the Ge and ZrO_2 references determined above.

Table 1 shows that both as-deposited pure 'Ge' and mixed 'Ge-ZrO_2' superlattice compositions can be equally well described by the single-layer (MsL) and multi-layer (MmL) models. The spectra fitted on sample 'Ge-ZrO_2' are shown in Fig. 5, revealing an acceptable fit quality. The amount of Ge is higher in the pure ('Ge') sample, as expected, but the fit did not result in a pure separate Ge layer.

Raman scattering spectra of as-deposited samples and samples annealed at $T_A < 650$ °C demonstrate a broad band corresponding to the amorphous Ge phase (left-hand side graph of Fig. 6). When T_A increases up to 700 °C, the Ge-related TO phonon shifts towards higher wavenumbers that is accompanied by its narrowing. The spectra of the samples annealed at $T_A = 700 - 800$ °C show a simultaneous presence of the bands from amorphous and crystalline Ge phases. This is therefore also included in the ellipsometric model denoted by 'c-Ge', as shown in Table 3.

The evolution of X-ray diffraction (XRD) patterns with annealing temperature (the right-hand side of Fig. 6) shows that phase decomposition occurs at first via the formation of the Ge phase. This is evident by the appearance of the Ge(111) peak and its narrowing with T_A rise. When Ge crystallites are formed, the crystallization of ZrO_2 sets in. The formation of tetragonal ZrO_2 phase is detected. The evolution of XRD patterns with temperature shows that the Ge and ZrO_2 phases crystallize at $T_A = 640 - 700$ °C and 700-800 °C, respectively. The comparison of the transformation of Raman scattering and XRD spectra with T_A allows to conclude the possibility

6

of Ge-NCs formation in the amorphous ZrO_2 host.

It is worth to note that the intensity of the XRD peaks related to the Ge phase decreases for the samples annealed at $T_A = 800$ °C that can be caused by the partial outward diffusion of Ge from the samples. This assumption was confirmed by the analysis of elemental depth-profile by means of Auger spectroscopy showed the lowering of Ge content in annealed Ge-rich-ZrO_2 single-layers. The average [Ge]/[Zr] ratio decreases from 0.75 (for as-deposited samples) to 0.57 (for annealed at 800 °C). This effect was found to be more prominent at the near-surface region, which is consistent with the MEIS results that also show a significant decrease of Ge content in those layers as a result of annealing, with a subsequent increase in the ZrO_2 sublayers (see Table 2). Taking into account the layer thicknesses, the total amount of Ge in all those measured layers also decreases. The decrease is 28% and 50% in the topmost and second 'ZrO_2 + Ge' sublayers, respectively, as also shown in the table.

The single-layer model applied for the annealed samples fails to describe the structure (see Fig. 8), due to the diffusion of elements, as revealed by MEIS and shown in Fig. 9 as well as in the Table 2. The deterioration cannot be explained by depolarization, because of the sub-wavelength size and uniform distribution of the formed grains (see the SEM inset in Fig. 6, as well as the small change in the depolarization, as shown in the bottom graph of Fig. 7).

Such outward Ge diffusion can result in the transformation of the structure of multi-stacked samples. Indeed, the ellipsometry results (see Table 3) show that the ratio of sub-layer thicknesses changes significantly with the annealing.

Multi-layer models (MmL) were also investigated (see Table 3), including a single-crystalline Ge component in the B-EMA, to account for the expected crystallization as shown by Fig. 6. The measured spectra revealed a substantial structural change as a function of the annealing (Fig. 7). In the multi-layer models, the sub-layer thicknesses as well as the volume fractions of the c-Ge and ZrO_2 phases have been fitted in a superlattice structure, i.e. each layer pair of Table 3 are repeated 40 times in the model, assuming a vertically uniform layer structure.

Considering the effect of annealing, a remarkable feature is the decrease of the mixed B-EMA sub-layer thickness, as well as the increase of the volume fraction of 'Ge' in this sublayer. The fit quality deteriorates above the annealing temperature of 650 °C with mean square error (MSE) values jumping

7

from 50 to over 200. It means that the fitted parameters for 700 and 750 °C cannot be considered as reliable. However, for the annealing temperatures of up to 650 °C, the above systematic changes of sub-layer thicknesses and 'Ge' ratio are consistent showing a phase separation with increasing annealing temperature.

The reason for the bad fit quality for the samples, annealed at $T_A >$ 650 °C, is most probably due to the vertical non-uniformity. This has also been justified by the MEIS results for the top three pairs of layers (Table 2) showing an increase of Ge content towards the surface. The attempt to construct optical models that take into account the vertical grading was not successful so far, because of the already large number of fit parameters.

One more source of possible errors is the difference between the dielectric function of forming cubic ZrO_2 and our reference (Fig. 3), however, only a minor change is expected in the used energy range [24]. It is important to note that in this study we only used the single-crystalline germanium component (c-Ge) to describe crystallinity, although we have shown before that in case of silicon a nanocrystalline component significantly improves the fit quality, because it describes the response of a material with a large number of grain boundaries, resulting in a broadening of the absorption peaks (due to the reduced lifetime of electrons scattered at the grain boundaries) [25, 26, 12]. The reason it was not used in this study is the lack of proper reference data. To obtain, model, parameterize and test those data requires more study, sample preparation and evaluations which could not be performed in frame of this work. However, even when using the c-Ge data instead should not significantly influence the tendencies and conclusions.

Conclusions

It has been shown that ellipsometry offers a characterization of Ge/ZrO_2 and Ge-rich-ZrO_2/ZrO_2 multi-layer structures with a high sensitivity. The as-deposited structure was successfully modeled using reference optical constants determined from single-layer characterizations. It has also been shown that the surface region (several layer-pairs from the top) can sensitively be measured be MEIS, that revealed substantial diffusion during annealing. Ellipsometry also shows a significant change in the measured spectra, however, the annealed sample (above the temperature of 700 °C) cannot be fitted with the assumption of a vertically uniform layer structure.

8

[1] S. Tiwari, F. Rana, H. Hanafi, A. Hartstein, E. Crabbé, K. Chan, A silicon nanocrystals based memory, Appl. Phys Lett. 68 (1996) 1377.

[2] H. Hanafi, S. Tiwari, I. Khan, Fast and long retention-time nano-crystal memory, IEEE Trans. Electron. Devices 43 (1996) 1553.

[3] E. Kapetanakis, P. Normand, D. Tsoukalas, K. Beltsios, Room-temperature single-electron charging phenomena in large-area nanocrystal memory obtained by low-energy ion beam synthesis, Appl. Phys.Lett. 80 (2002) 2794.

[4] L. Khomenkova, B. Sahu, A. Slaoui, F. Gourbilleau, Hf-based high-k materials for Si nanocrystal floating gate memories, Nanoscale Res. Lett. 6 (2011) 172.

[5] G. Conibeer, M. Green, R. Corkish, Y. Cho, E. Cho, C. Jiang, T. Fang-suwannarak, E. Pink, Y. Huang, T. Puzzer, Silicon nanostructures for third generation photovoltaic solar cells, Thin Solid Films 511-512 (2006) 654.

[6] M. Fujii, M. Yoshida, S. Hayashi, K. Yamamoto, Photoluminescence from SiO_2 films containing Si nanocrystals and Er: Effects of nanocrystalline size on the photoluminescence efficiency of Er^{3+}, J. Appl. Phys. 84 (1998) 4525.

[7] V. Timoshenko, M. Lisachenko, O. Shalygina, B. Kamenev, D. Zhigunov, S. Teterukov, P. Kashkarov, J. Heitmann, M. Schmidt, M. Zacharias, Comparative study of photoluminescence of undoped and erbium-doped size-controlled nanocrystalline Si/SiO_2 multilayered structures, J. Appl. Phys. 96 (2004) 2254.

[8] L. Pavesi, L. D. Negro, C. M. G. Franzò, F. Priolo, Optical gain in silicon nanocrystals, Nature 408 (2000) 440.

[9] D. Lehninger, P. Seidel, M. Geyer, F. Schneider, V. Klemm, D. Rafaja, J. von Borany, J. Heitmann, Charge trapping of Ge-nanocrystals embedded in $TaZrO_x$ dielectric films, Appl. Phys. Lett. 106 (2015) 23116.

9

[10] D. Lehninger, L. Khomenkova, C. Röder, G. Gärtner, B. Abendroth, J. B. F. Schneider, D. C. Meyer, J. Heitmann, Ge nanostructures embedded in ZrO_2 dielectric films for nonvolatile memory applications, ECS Transactions 66 (2015) 203.

[11] P. Petrik, M. Fried, Ellipsometry of Semiconductor Nanocrystals, in: M. Losurdo, K. Hingerl (Eds.), Ellipsometry at the Nanoscale, Springer-Verlag, Heidelberg, 2012, p. 583.

[12] P. Petrik, M. Fried, E. Vazsonyi, P. Basa, T. Lohner, P. Kozma, Z. Makkai, Nanocrystal characterization by ellipsometry in porous silicon using model dielectric function, Journal of Applied Physics 105 (2009) 024908.

[13] E. Agocs, A. G. Nassiopoulou, S. Milita, P. Petrik, Model dielectric function analysis of the critical point features of silicon nanocrystal films in a broad parameter range, Thin Solid Films 541 (2013) 83–86.

[14] P. Petrik, Characterization of Nanocrystals Using Spectroscopic Ellipsometry, in: S. Neralla (Ed.), Nanocrystals - Synthesis, Characterization and Applications, InTech, 2012.

[15] E. Kótai, Computer methods for analysis and simulation of rbs and erda spectra, Nucl. Instr. and Meth. B85 (1994) 588.

[16] C. M. Herzinger, B. Johs, W. A. McGahan, J. A. Woollam, W. Paulson, Ellipsometric determination of optical constants for silicon and thermally grown silicon dioxide via a multi-sample, multi-wavelengt, multi-angle investigation, J. Appl. Phys. 83 (1998) 3323.

[17] M. Fried, T. Lohner, W. A. M. Aarnink, L. J. Hanekamp, A. van Silfhout, Determination of complex dielectric functions of ion-implanted and implanted-annealed silicon by spectroscopic ellipsometry, J. Appl. Phys. 71 (1992) 5260.

[18] S. Adachi, H. Mori, Optical properties of fully amorphous silicon, Physical Review B 62 (2000).

[19] A. M. Antoine, B. Drevillon, P. R. i Cabarrocas, In situ investigation of the growth of rf glow-discharge deposited amorphous germanium and silicon films, Journal of Applied Physics 61 (1987) 2501.

10

[20] O. W. Holland, B. R. Appleton, J. Narayan, Ion implantation damage and annealing in germanium, Journal of Applied Physics 54 (1983) 2295.

[21] A. A. Al-Mahasneh, H. A. Al Attar, I. S. Shahin, Spectroscopic ellipsometry of single and multilayer amorphous germanium/aluminum thin film systems, Optics Communications 220 (2003) 129.

[22] M. M. Giangregorio, M. Losurdo, M. Ambrico, P. Capezzuto, G. Bruno, L. Tapfer, Dielectric function and electric properties of germanium thin films prepared by gold mediated crystallization, Journal of Applied Physics 99 (2006) 063511.

[23] E. S. M. Goh, C. Q. Sun, Y. C. Liu, Thickness effect on the band gap and optical properties of germanium thin films, Journal of Applied Physics 107 (2010) 024305.

[24] J. C. Garcia, L. M. R. Scolfaro, A. T. Lino, V. N. Freire, G. A. Farias, C. C. Silva, H. W. Leite Alves, S. C. P. Rodrigues, E. F. da Silva Jr., Structural, electronic, and optical properties of ZrO_2 from ab initio calculations, Journal of Applied Physics 100 (2006) 104103–1.

[25] P. Petrik, M. Fried, T. Lohner, R. Berger, L. P. Biró, C. Schneider, J. Gyulai, H. Ryssel, Comparative study of polysilicon-on-oxide using spectroscopic ellipsometry, atomic force microscopy, and transmission electron microscopy, Thin Solid Films 313-314 (1998) 259.

[26] P. Petrik, T. Lohner, M. Fried, L. P. Biró, N. Q. Khánh, J. Gyulai, W. Lehnert, C. Schneider, H. Ryssel, Ellipsometric study of polycrystalline silicon films prepared by low pressure chemical vapor deposition, Journal of Applied Physics 87 (2000) 1734.

[27] R. A. Synowicki, T. E. Tiwald, Optical properties of bulk c-ZrO_2, c-MgO and a-As_2S_3 determined by variable angle spectroscopic ellipsometry, Thin Solid Films 455-456 (2004) 248–255.

[28] S. Adachi, Optical Constants of Crystalline and Amorphous Semiconductors, Numerical Data and Graphical Information, Kluwer Academic Publishers, 1999.

11

[29] D. E. Aspnes, A. A. Studna, Dielectric functions and optical parameters of Si, Ge, GaP, GaAs, GaSb, InP, InAs, and InSb from 1.5 to 6.0 eV, Physical Review B 27 (1983) 985–1009.

12

Table 1: Fitted parameters of the ellipsometric evaluation on the as-deposited samples. d_{ox} and d_t denote the thickness of the capping oxide and the total thickness, respectively. 'Ge' is the reference (see Fig. 4) determined from the single-layer sample. MSE denotes the mean square error of the fit. The confidence limits for the fit on d_{ox}, d_t and the volume fractions of the components are below 0.2 nm, 0.5 nm, and 0.5%, respectively.

Sample	Model	d_{ox} (nm)	Composition	d_t (nm)	MSE
'Ge'	MsL	26.3	361 nm (47.7% Ge + 52,3% ZrO_2)	361	18
'Ge'	MmL	21	4.4 nm (100% ZrO_2)×41 4.9 nm (69.7% Ge + 30.3% ZrO_2)×40	376.8	11
'Ge-ZrO_2'	MsL	24	435.2 nm (14.4% Ge + 85.6% ZrO_2)	435.2	39
'Ge-ZrO_2'	MmL	22.1	4 nm (100% ZrO_2)×41 7 nm (20% Ge + 80% ZrO_2)×40	440.4	38

Table 2: Sublayer depths and atomic compositions ($Ge_x ZrO_2$) measured by MEIS on Sample 'Ge-ZrO_2'. For the annealed sample the sublayer thicknesses were not changed with respect to the reference, only the Ge contents in the sublayers have been varied. The relative error of the parameters measured by MEIS is approximately 10%.

Layer	Thickness (10^{16} at/cm^2)	Ge content (x) As-deposited	Annealed
SiO_2	10.5	0.08	0.08
ZrO_2	3.5	0.5	0.9
ZrO_2 + Ge	4.7	1.8	1.3
ZrO_2	3	0.4	0.9
ZrO_2 + Ge	3.7	1.6	0.8
ZrO_2	3	0.0	0.45

13

Table 3: Fitted parameters of model 'MmL' on the sample annealed at 600-750 °C. d_{ox} and d_t denote the thickness of the capping oxide and the total thickness, respectively. MSE stands for the mean square error of the fit.

T (°C)	d_{ox} (nm)	Composition	d_t (nm)	MSE
-	19.6±0.1	7.8±0.1 nm (100% ZrO$_2$)×41 3.1±0.1 nm (14.6±0.4% Ge + 23.4±0.4% c-Ge + 62±0.8% ZrO$_2$)×40	445	28
600	19.8±0.1	8.1±0.1 nm (100% ZrO$_2$)×41 2.5±0.1 nm (25.9±0.5% Ge + 22.7±0.9% c-Ge + 51.4±1% ZrO$_2$)×40	431.7	26
650	25.8±0.3	10.2±0.1 nm (100% ZrO$_2$)×41 0.7±0.1 nm (100±12% Ge + 0% c-Ge + 0±12% ZrO$_2$)×40	446.6	47
700	28.6±1.1	10.3±0.3 nm (100% ZrO$_2$)×41 0.7±0.2 nm (74.6±15% Ge + 0±7% c-Ge + 25.4±16.4% ZrO$_2$)×40	449.1	236
750	16.2±0.9	9±0.30 nm (100% ZrO$_2$)×41 1.6±0.30 nm (34±3.6% Ge + 1.0±3.8% c-Ge + 65±5.2% ZrO$_2$)×40	432.2	196
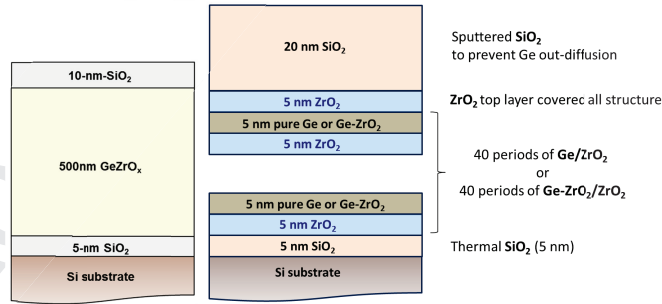
Figure 1: Schematic illustration of Ge-ZrO$_2$ mixed-phase single-layer (left-hand side) and multi-layer (right-hand side) structures prepared by confocal radio frequency magnetron sputtering [9].

14
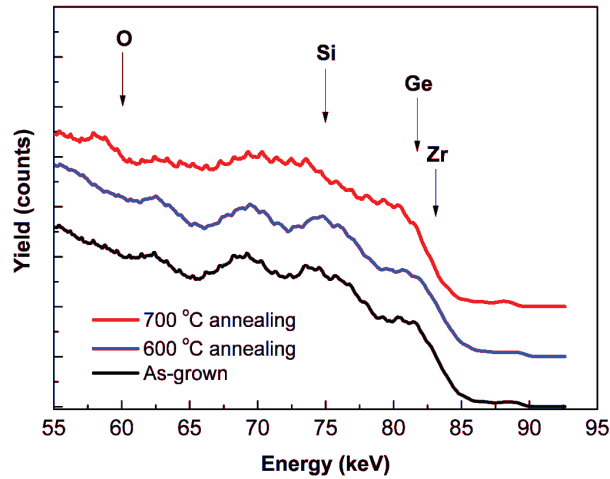
Figure 2: MEIS spectra measured with 100 keV He$^+$ analizing ions at a scattering angle of 90° and at a sample tilt angle of 54.7° with respect to the ion beam. The spectrum edges of Zr and Ge in the first and second sublayer as well as Si and O in the surface silicon dioxide layer are indicated by arrows.
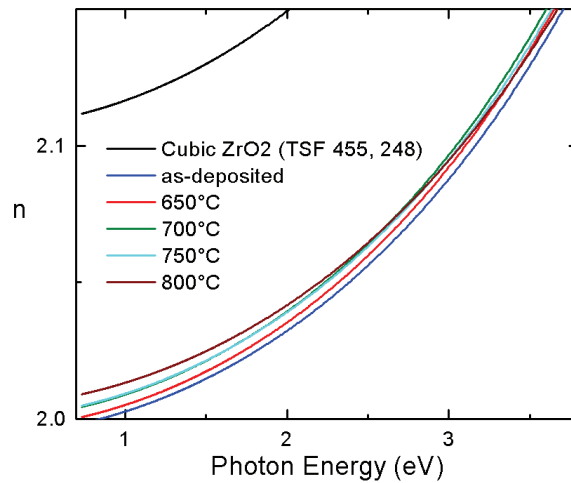

Figure 3: Optical properties of ZrO_2 extracted for single-layer sample without and with annealing at different temperatures. The reference for cubic ZrO_2 is also plotted [27].
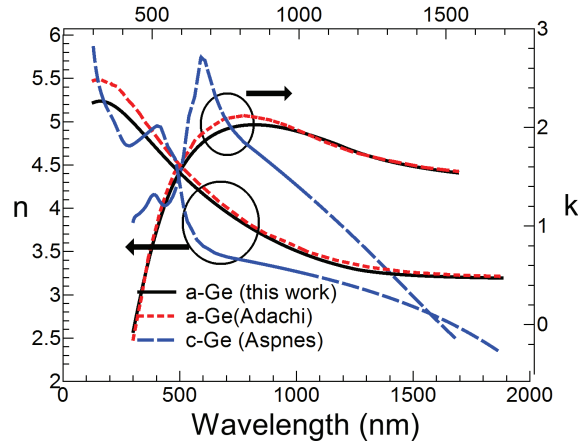
15

Figure 4: Optical properties of as-deposited Ge extracted for a single-layer sample deposited using the same parameters as for the multi-layer structures, together with amorphous (a-Ge, Ref. [28]) and single-crystalline (c-Ge, Ref. [29]) references. The fit results for the as-deposited Ge are $E_g = 0.76 \pm 0.01$ eV, $A = 88.4 \pm 0.4$ eV, $E_0 = 3.4 \pm 0.01$ eV, $\Gamma = 4.41 \pm 0.02$ eV, $E_p = 0.66 \pm 0.01$ eV, $E_t = 0.28 \pm 0.01$ eV, and $E_u = 0.14 \pm 0.01$ eV, $\epsilon_{inf} = 1.9 \pm 0.02$ eV.
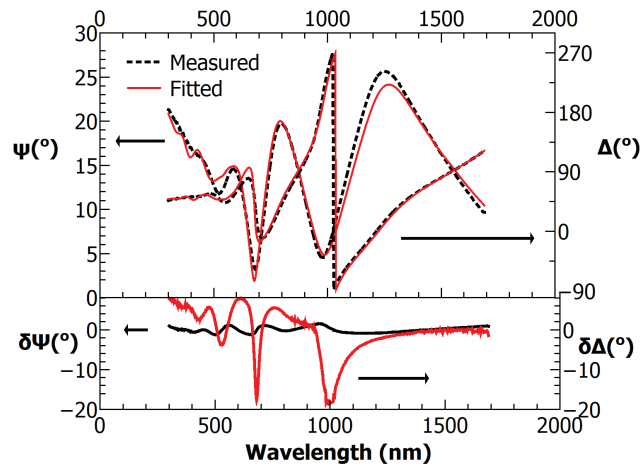

Figure 5: Measured and fitted spectra for the as-deposited sample of 'Ge-ZrO$_2$' using the single-layer (MsL) model. The bottom graph shows the differences between the measured and fitted Ψ and Δ spectra. The angle of incidence was 70°.
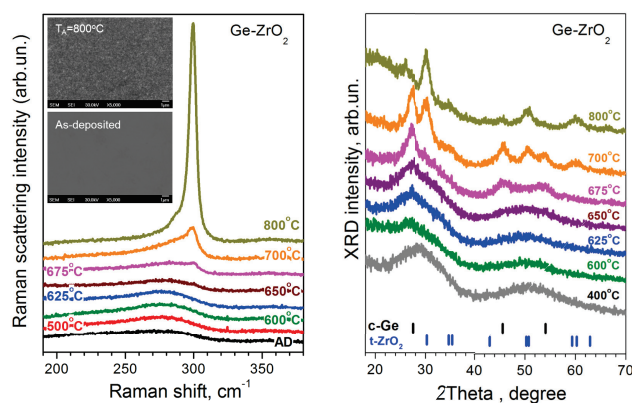
16

Figure 6: Raman scattering spectra (left) and XRD patterns (right) of Ge-rich-ZrO$_2$ single-layer films for annealing temperatures up to 800 °C. The inset in the top-left corner of the left-hand graph show scanning electron microscopy (SEM) images on as-deposited and annealed samples.
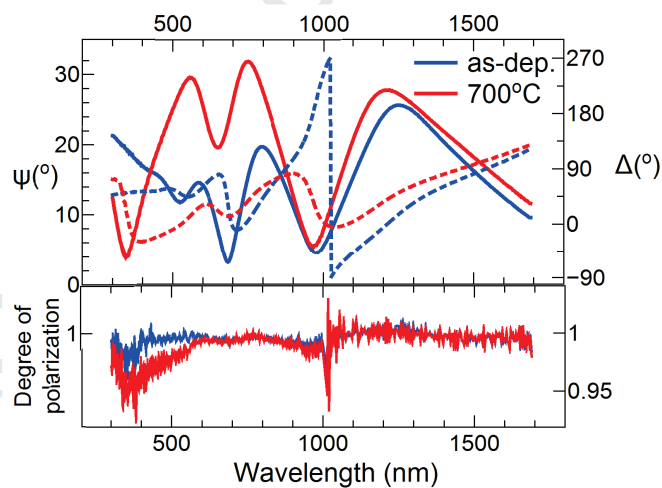

Figure 7: Measured Ψ (solid lines) and Δ (dashed lines) spectra for Sample 'Ge-ZrO$_2$' annealed at 700 °C (red lines) as well as without annealing (blues lines, 'as-dep.'). The angle of incidence was 70°.
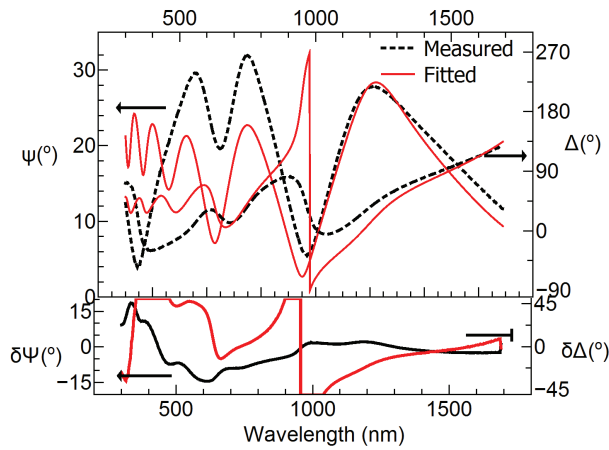
17

Figure 8: Measured and fitted spectra using the single-layer model (MsL) for Sample 'Ge-ZrO$_2$' annealed at 700 °C. The angle of incidence was 70°.
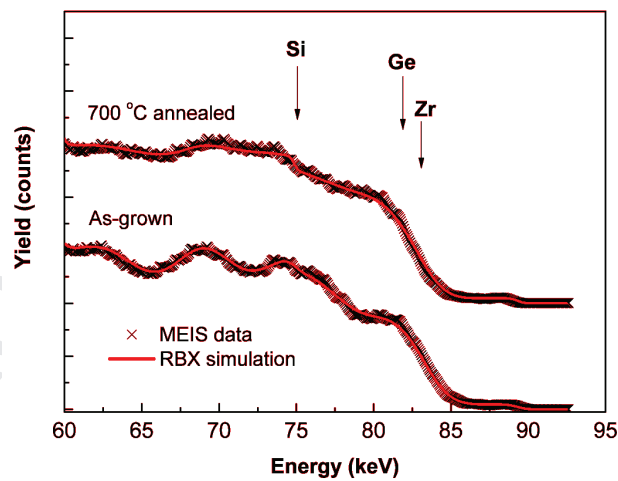

Figure 9: MEIS spectra and the corresponding RBX simulations of as-deposited and annealed 'Ge-ZrO$_2$' samples. The spectrum edges of Zr and Ge in the first and second sublayer as well as Si in the surface silicon dioxide layer are indicated by arrows.

18